

# An activating germline *IDH1* variant associated with a tumor entity characterized by unilateral and bilateral chondrosarcoma of the mastoid

Patrick R. Blackburn,<sup>1,2,3,18,19</sup> Jodi M. Carter,<sup>3,19,\*</sup> Devin Oglesbee,<sup>3,4</sup> Jennifer J. Westendorf,<sup>5,6</sup> Brian A. Neff,<sup>7</sup> Damian Stichel,<sup>8,9</sup> David W. Tsen,<sup>10</sup> Ralitzia H. Gavrilova,<sup>4,11</sup> Pieter Wesseling,<sup>12,13,14</sup> Andreas von Deimling,<sup>8,9</sup> Thomas R. Caulfield,<sup>15,16,17</sup> Eric W. Klee,<sup>1,2,3,4</sup> Stefan Pusch,<sup>8,9,\*</sup> and Carrie Y. Inwards<sup>3,5</sup>

## Summary

Chondrogenic tumors involving the temporal bone are rare and typically arise spontaneously with unilateral presentation. Somatic *IDH* mutations are common in these tumors, but germline inheritance has not been documented to our knowledge. We describe familial chondrosarcoma, grade 1, of the mastoid with unilateral presentation in the mother and bilateral presentation in each of her two children. Each individual presented with headaches, facial paresis, and conductive hearing loss between the ages of 9–12. Exome sequencing of all three affected family members identified a shared germline heterozygous c.299G>A (p.Arg100Gln) missense variant in *IDH1*. The p.Arg100Gln variant has only rarely been observed as a somatic mutation in glial tumors, and previous *in vitro* experiments have shown that p.Arg100Gln produces small amounts of the oncometabolite D-2-hydroxyglutarate (D2HG). Biochemical testing in all three affected family members on urine and plasma was unable to detect increases in D2HG in these sample types. Due to insufficient tumor for methylation studies, we performed genome-wide methylation analysis of an *IDH1* p.Arg100Gln mutant brain tumor from an unrelated individual to functionally evaluate this variant. These studies demonstrated a global hypermethylation phenotype consistent with other known isocitrate dehydrogenase (IDH) mutant brain tumors, suggesting that this variant has neomorphic activity despite low-level production of D2HG. The bones of the facial skeleton are formed by membranous ossification and we hypothesize that abnormal embryonic cartilage that rests within the suture lines may be involved in this tumor entity. Testing of additional individuals with similar presentations is needed to confirm this finding and clarify the associated phenotypes.

Isocitrate dehydrogenase 1 (IDH1) and IDH2 are homodimeric nicotinamide adenine dinucleotide phosphate (NADP)-dependent enzymes that catalyze the oxidative decarboxylation of isocitrate into alpha-ketoglutarate ( $\alpha$ -KG), the third step of the Krebs cycle.<sup>1</sup> IDH1 is primarily localized to the cytosol and peroxisomes, while IDH2 is found mainly within mitochondria. Both IDH1 and IDH2 have influence on the epigenetic state of cells through the production of  $\alpha$ -KG, which is utilized by many  $\alpha$ -KG-dependent dioxygenases, such as DNA and histone demethylases. Several recurrent somatic variants in these enzymes have been observed in homologous residues within the active sites of both enzymes that confer neomorphic activity with the production of D-2-hydroxyglutarate (D2HG).<sup>1</sup> D2HG acts as an oncometabo-

lite and may play a role in tumor development through global dysregulation of the epigenetic environment in cells.

In addition to subsets of cartilaginous tumors, somatic gain-of-function variants in *IDH1* (MIM: 147700) and *IDH2* (MIM: 147650) occur frequently in acute myeloid leukemias, myelodysplastic syndromes, angioimmunoblastic T cell lymphomas, thyroid carcinomas, cholangiocarcinomas, and gliomas.<sup>2</sup> While primary cartilage-forming tumors are rare, enchondromas are the most common benign tumors of bone and conventional chondrosarcoma is the most common malignant cartilaginous tumor of bone. The vast majority of enchondromas and conventional chondrosarcomas are sporadic events; however, some are syndromic.<sup>3</sup> Both simplex and syndromic

<sup>1</sup>Center for Individualized Medicine, Mayo Clinic, Rochester, MN 55905, USA; <sup>2</sup>Department of Health Sciences Research, Mayo Clinic, Rochester, MN 55905, USA; <sup>3</sup>Department of Laboratory Medicine and Pathology, Mayo Clinic, Rochester, MN 55905, USA; <sup>4</sup>Department of Clinical Genomics, Mayo Clinic, Rochester, MN 55905, USA; <sup>5</sup>Department of Orthopedic Surgery, Mayo Clinic, Rochester, MN 55905, USA; <sup>6</sup>Department of Biochemistry and Molecular Biology, Mayo Clinic, Rochester, MN 55905, USA; <sup>7</sup>Department of Otolaryngology-Head and Neck Surgery, Mayo Clinic, Rochester, MN 55905, USA; <sup>8</sup>German Consortium of Translational Cancer Research (DKTK), Clinical Cooperation Unit Neuropathology, German Cancer Research Center (DKFZ), Heidelberg 69120, Germany; <sup>9</sup>Department of Neuropathology, Institute of Pathology, Ruprecht-Karls-University Heidelberg, Heidelberg 69120, Germany; <sup>10</sup>Department of Otolaryngology, Essentia Health, Fargo, ND 58103, USA; <sup>11</sup>Department of Neurology, Mayo Clinic, Rochester, MN 55905, USA; <sup>12</sup>Department of Pathology, Cancer Center Amsterdam, VU University Medical Center, Amsterdam 1081 HV, the Netherlands; <sup>13</sup>Brain Tumor Center Amsterdam, VU University Medical Center, Amsterdam 1081 HV, the Netherlands; <sup>14</sup>Department of Pathology, Princess Máxima Center for Pediatric Oncology and University Medical Center Utrecht 3584 EA, the Netherlands; <sup>15</sup>Department of Neuroscience, Mayo Clinic Florida, Jacksonville, FL 32224, USA; <sup>16</sup>Department of Health Sciences Research, Mayo Clinic Florida, Jacksonville, FL 32224, USA; <sup>17</sup>Department of Cancer Biology, Mayo Clinic Florida, Jacksonville, FL 32224, USA

<sup>18</sup>Present address: Department of Pathology, St. Jude Children's Research Hospital, Memphis, TN 38105, USA

<sup>19</sup>These authors contributed equally to this work

\*Correspondence: [carter.jodi@mayo.edu](mailto:carter.jodi@mayo.edu) (J.M.C.), [stefan.pusch@med.uni-heidelberg.de](mailto:stefan.pusch@med.uni-heidelberg.de) (S.P.)

<https://doi.org/10.1016/j.xhgg.2020.100006>.

© 2020 This is an open access article under the CC BY-NC-ND license (<http://creativecommons.org/licenses/by-nc-nd/4.0/>).



cartilaginous tumors frequently harbor somatic *IDH* mutations.

In *IDH1*, the Arg132 residue that is mutated in a majority of tumors is homologous to the Arg172 residue in *IDH2*, while the Arg140 residue in *IDH2* is homologous to Arg100 in *IDH1*. Somatic heterozygous variants in *IDH1* and *IDH2* are frequently seen in several syndromes associated with formation of multiple cartilaginous tumors, including Ollier disease (MIM: 166000), Maffucci syndrome (MIM: 614569), and metaphyseal enchondromatosis with urinary excretion of D-2-hydroxyglutaric acid (MIM: 614875).<sup>4,5</sup> Individuals with these disorders have multiple enchondromas and an increased risk of chondrosarcoma and other malignancies, including gliomas.<sup>6</sup> The *IDH2* p.Arg140Gln variant is also the most common germline variant identified in individuals with autosomal dominant D-2-hydroxyglutaric aciduria-2 (D2HGA2; MIM: 613657), a severe disorder characterized by developmental delay, epilepsy, hypotonia, cardiomyopathy, dysmorphic features, and early lethality.<sup>5</sup> The *IDH1* p.Arg100Gln variant has been reported rarely (<1%) in a spectrum of glial tumors: low-grade gliomas, recurrent glioblastomas, anaplastic oligodendrogliomas, and astrocytomas.<sup>7,8</sup> To date, *IDH1* p.Arg100Gln has not been reported in cartilaginous tumors, and no germline disorders have been associated with variants in *IDH1*.

Herein, we describe a family with three members presenting in early adolescence with chondrosarcoma, grade 1 involving the mastoid portion of the temporal bone. Notably, two of the three affected members had bilateral presentation. Cartilaginous tumors arising in the mastoid bone are rare, and there have been no described cases of bilateral cartilaginous tumors at this site to our knowledge. Conventional cytogenetic analysis performed on the proband revealed no clonal abnormalities. In addition, high-resolution array comparative genomic hybridization (aCGH) performed on the individual's blood showed no evidence of a germline abnormality. Due to the relative rarity of the tumor type, the unusual bilateral presentation, restricted anatomical location, and evidence of tumors in at least two generations within this family, a genetic disorder was suspected. Whole exome sequencing (WES) was performed on blood from the proband, mother, father, and the proband's half-brother, identifying a heterozygous missense variant in *IDH1* (GenBank: NM\_005896.4, c.299G>A; NCBI: NP\_005887.2, p.Arg100Gln) that was unique to the three affected individuals.

All study participants provided written informed consent for sample collection and subsequent analysis under a protocol approved by the institutional review board of the Mayo Clinic. The family in this report has been previously described.<sup>9</sup> The 9-year-old male proband (individual II-1, Figure 1A) presented with a history of bilateral conductive hearing loss and had developed right facial paresis. Computed tomography (CT) revealed a mass involving the mastoid (Figure 1B), and the proband underwent a right tympanomastoidectomy. A CT scan of the

temporal bone on the left side showed opacification of the mastoid air cells and most of the middle ear, with demineralization of the mastoid matrix. There was also thinning of the lateral wall of the jugular foramen, suggestive of an erosive expansile process in the mastoid that involved the jugular bulb (Figure 1C). A magnetic resonance image (MRI) of the skull base demonstrated a left-sided peripherally enhancing mass within the mastoid adjacent to the mastoid segment of the facial nerve (Figure 1D). The proband had a left tympanomastoidectomy and complete tumor resection on the left ear 6 months later (Figure 1E). Histologic analysis revealed a hypo- to moderately cellular hyaline cartilage tumor with areas of host bone entrapment, consistent with a grade 1 (low-grade) chondrosarcoma (Figures 1F and 1G). Conventional cytogenetics analysis revealed no clonal abnormality within the proband's tumor.

The proband's 11-year-old half-brother (individual II-2, Figure 1A) similarly developed left facial nerve paralysis and underwent a left-sided mastoidectomy for tumor resection. Repeat CT scan showed an abnormality on the contralateral right side, and a tumor involving the mastoid and antrum was removed (Figure 1H). The brothers did not receive postoperative treatment, and there has been no evidence of recurrence to date based on serial MRI scans. The mother of both children also had a history of facial nerve dysfunction and mastoid tumor at 12 years of age. The mother had a left radical mastoidectomy (Figure 1I) and received postoperative radiation and chemotherapy. External pathologic review of the tumor rendered a diagnosis of a well-differentiated low-grade chondrosarcoma. The mother has had no recurrence of disease to date.

The proband's mother (individual I-2, Figure 1A) had a limited genetics evaluation at 35 years of age. In addition to having a history of malignancy, the mother reported childhood seizures, three stroke-like episodes, and recurrent infections. On evaluation, she had slightly dysmorphic features, including a short nose, upturned nostrils, arched eyebrows, and small chin with a head circumference of 59.2 cm (>99 percentile [+4.4 SD]). Both the proband and his half-brother had a small chin, similar to the mother, and were normocephalic. The proband was also noted to have somewhat dysmorphic facial features, with a flat blunted forehead and a widened face. Complete skeletal surveys were performed on all three individuals and showed no other bony abnormalities.

Based on the presence of cartilaginous tumors in three family members from two generations, an autosomal dominant or X-linked genetic disorder was suspected. For WES, DNA was extracted from blood from the proband, mother, father, and proband's half-brother. The Agilent SureSelect Human All Exon V5+UTR WES capture kit was utilized for this study. The GenomeGPS pipeline (formerly TREAT) was used for alignment and analysis.<sup>10</sup> From the Illumina HiSeq platform, 100-bp paired end reads were aligned to hg19 using Novoalign (Novocraft Technologies, Malaysia). The quality of sequencing chemistry was evaluated using

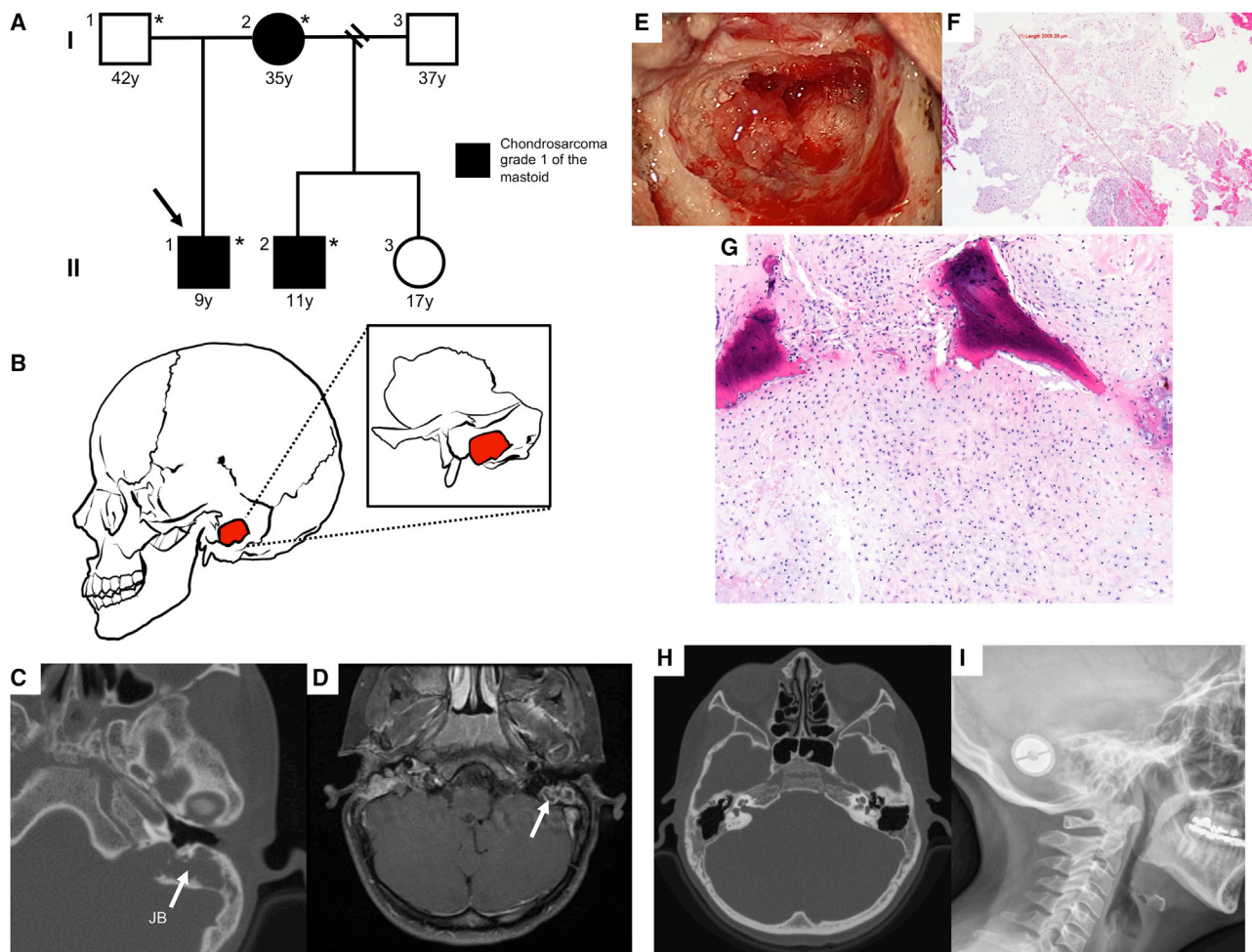


**Figure 1. Overview of the Clinical and Pathological Presentation of Mastoid Lesions in the Described Family**

(A) Pedigree showing the presence of mastoid lesions across two generations. Numbers under the symbols indicate ages at last evaluation. Shading indicates the presence of the phenotype. Asterisks indicate individuals who had whole-exome sequencing performed. The arrow indicates the proband.

(B) Diagram showing the location of the mastoid; zoomed-in cutout of the temporal bone, with the mastoid portion shown in red.

(C) Axial, non-contrast CT of temporal bone for the proband. The mass (white arrow) fills the left mastoid with erosion of bony septae and bone over the jugular bulb (JB).

(D) Axial gadolinium-enhanced MRI of the skull base for the proband. MRI demonstrates a heterogeneously enhancing mass (white arrow) within the left mastoid without intracranial extension. The contralateral right mastoid shows post-surgical scar tissue.

(E) Intraoperative view of chondrosarcoma, grade 1 within the mastoid extending into the antrum, facial recess, and retrofacial air cell tract.

(F) Chondrosarcoma, grade 1, demonstrating mild hypercellularity and (G) host bone entrapment.

(H) Head CT of the proband's half-brother after bilateral mastoidectomy with opacification.

(I) Recent skull radiographs of proband's mother showing lateral view with metallic device over the left occiput.

FastQC, and realignment and recalibration steps were performed using GATK.<sup>11</sup> All germline variants were jointly called through GATK Haplotype Caller with PhaseByTransmission enabled and GenotypeGVCF. Variant quality score recalibration (VQSR) filters were applied based on GATK best practices. Each variant was annotated using the BioR Toolkit.<sup>12</sup> The annotated variant call format file was loaded into QIAGEN's Ingenuity Variant Analysis software (QIAGEN, Redwood City) for causal variant identification (see [Supplemental material and methods](#)).

Starting with 156,698 variants spanning 27,059 genes, variant filtering was performed to generate a list of candidate disease-associated variants: (1) due to the rarity of

this tumor type and absence of familial cases in the literature, population-based filtration removed variants present at a general population allele frequency greater than or equal to 0.01% in ExAC or greater than or equal to 0.01% in gnomAD (overall population max frequency) unless it was an established pathogenic common variant; (2) the functional impact-based filtration kept variants that were pathogenic, possibly pathogenic, or disease-associated according to the Human Gene Mutation Database (HGMD) as well as any frameshift, in-frame indel, nonsense, missense, variants predicted to disrupt splicing by MaxEntScan, or which occurred within 4 bases into the intron; and (3) inheritance-based filters were used to

remove variants that did not segregate in all three affected family members or that were present in the unaffected father (i.e., consistent with autosomal dominant inheritance pattern).

The differential diagnosis included autosomal dominant multiple exostoses syndrome type I and type II that is caused by variants in *EXT1* (MIM: 133700) and *EXT2* (MIM: 133701). Chondrosarcomas have also been described in Li-Fraumeni syndrome due to variants in *TP53* and *CHEK2* genes (MIM: 151623 and 609265). Heterozygous mutations in *PTPN11* have also been associated with autosomal dominant metachondromatosis (MIM: 151623).<sup>13,14</sup> No variants in *EXT1*, *EXT2*, *PTPN11*, *TP53*, or *CHEK2* were found in any of the affected individuals. Only 49 variants met our strict filtering criteria (Table S1). Phased germline variants were evaluated for clinical relevance by a multidisciplinary team of clinicians and researchers and categorized according to American College of Medical Genetics (ACMG) guidelines, which identified only a single reportable missense variant in exon 4 of *IDH1* [Chr2(GRCh37): g.209113208C>T; GenBank: NM\_005896.4, c.299G>A; GenBank: NP\_005887.2, p.Arg100Gln]. The read depth was >275 in all cases, and the c.299G>A alternative allele fraction ranged from 46% to 53% (Table S1). 97%–98% of the target exome was covered at a read depth of 40× or greater (Table S2).

The p.Arg100Gln variant has not been observed in gnomAD but has been reported in COSMIC. Two variants are present at this codon in gnomAD, including a nonsense variant [Chr2(GRCh37): g.209113209G>A; GenBank: NM\_005896.4: c.298C>T; GenBank: NP\_005887.2: p.Arg100Ter] present in one Latino, one South Asian, and one European (non-Finnish) individual and a synonymous variant [Chr2(GRCh37): g.209113209G>T; GenBank: NM\_005896.4, c.298C>A; GenBank: NP\_005887.2, p.Arg100 = ] present in three Latino individuals. The family in this study is white with mixed European ancestry on both the maternal and paternal sides. The Arg100 residue is completely conserved across species and is conserved in lower eukaryotes, including yeast (*Saccharomyces cerevisiae*), and the p.Arg100Gln variant is homologous to the *IDH2* p.Arg140Gln variant (Figure 2A). The missense variant is predicted to be deleterious by SIFT, probably damaging by PolyPhen-2, and has a combined annotation dependent depletion (CADD) score of 35.<sup>15–17</sup> According to ACMG 2015 criteria, the variant was classified as a variant of uncertain significance (VUS).

To understand the activation mechanisms of *IDH1*, including its native conformations and impact of the p.Arg100Gln variant on enzyme function, we performed molecular modeling and dynamics simulations. *In silico* models were generated primarily from X-ray data sources and refined using a combination of methods, including Psi-pred, homology, secondary structure prediction, *ab initio* calculations, and arrays composite structure overlay, for threading (see Supplemental material and methods).

The oxidative decarboxylation of isocitrate to  $\alpha$ -KG is a two-step process in which *IDH1* adopts a closed conformation during binding of the isocitrate substrate complex (including NADP<sup>+</sup> and Mg<sup>2+</sup>) between large and small domains of the enzyme. Overall conformational differences throughout simulations were summarized using root mean square deviation (RMSD) measurements. These calculations for *IDH1* wild type (WT) and the p.Arg100Gln protein variant (Figure 2B) showed more global RMSD over time than WT. The increase in RMSD overall was minimal, since both structures are stable in dimeric form, but there are consistently larger global changes in p.Arg100Gln. We also examined WT and p.Arg100Gln variant dimers for hydrogen bond content as a determinate of inter-monomer stability. Interestingly, p.Arg100Gln has more hydrogen bonds between the interfaces of this tightly packaged dimer than the WT. The average hydrogen bond content is 17 and 14 for p.Arg100Gln and WT, respectively. It is possible that the increased stability in the interface of the enzymes is antagonizing the enzymatic activity and lowering catalysis efficiency, which comes via coordinated interactions across the enzyme via the backbone dihedrals. We find that *IDH1* p.Arg100Gln has several coordinated fluctuations across the dimeric *IDH1* enzyme that arise from both dimer interface interactions (Figure 2B) and inter-monomer changes via correlated dihedrals that allow for deleterious changes in the variant (p.Arg100Gln), which likely lower its catalytic efficiency compared to WT.

We next wanted to examine local changes within the catalytic site of variant *IDH1* (Figure 2C). The active site is composed of two essential catalytic residues, Tyr140 and Lys212, that participate in catalysis during decarboxylation of isocitrate and a triad of arginine residues, Arg100, Arg109, and Arg132, in the substrate recognition site that form a salt-bridge with isocitrate (Figure 2C).<sup>18</sup> Within the substrate recognition site, Arg132 forms three hydrogen bonds with the  $\alpha$ - and  $\beta$ -carboxyl of isocitrate, while Arg100 forms two bonds and Arg109 forms a single bond.<sup>18</sup> Modeling studies in *IDH1* suggest that substitutions at Arg132 would impair the enzyme substrate interactions, which is supported by studies of enzyme kinetics.<sup>19,20</sup> We used FoldX to calculate quantitative estimates of protein interface energies for the substrate complex for both WT and p.Arg100Gln *IDH1*. The WT energy was calculated to be  $-52.77$  kcal/mol, while the p.Arg100Gln variant had a predicted energy of  $-50.57$  kcal/mol with a net difference ( $\Delta G$ ) =  $-2.77$  kcal/mol, which is consistent with the loss of hydrogen bonds in the p.Arg100Gln catalytic site, leading to a decrease in the strength of attraction between *IDH1* and the isocitrate substrate complex. Compared to *IDH2* WT and the homologous variant p.Arg140Gln (Figure 2C), similar changes were observed (WT =  $-73.84$  kcal/mol; p.Arg140Gln =  $-71.99$  kcal/mol; net difference ( $\Delta G$ ) =  $-1.85$  kcal/mol). These findings

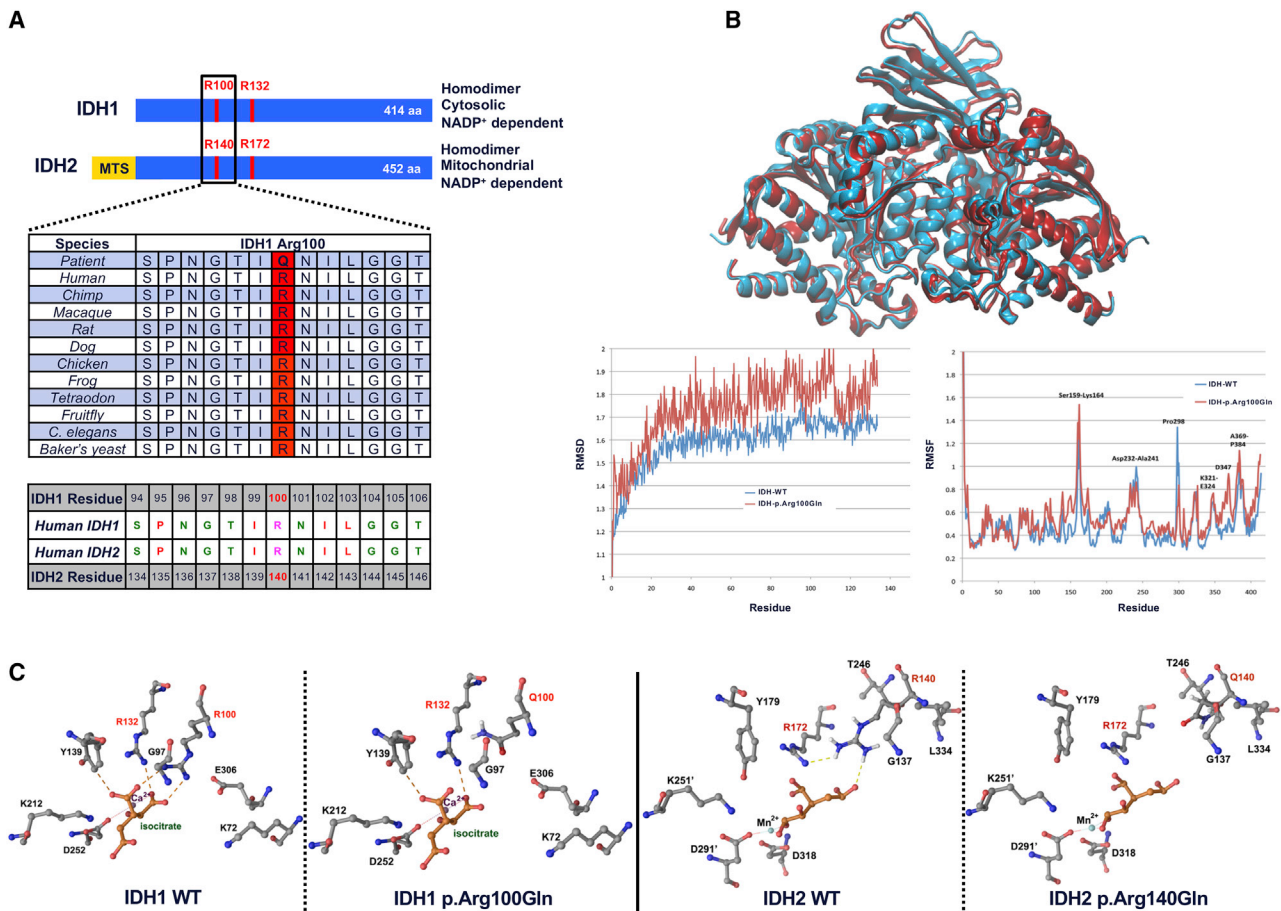


**Figure 2. Graphic Representation of IDH1 and IDH2 Variants and Results of Modeling and Dynamics Simulations**

(A) Schematic diagram of the protein structure of IDH1 (GenBank: NP\_005887.2) and IDH2 (GenBank: NP\_002159.2) showing homologous residues that are recurrently mutated and result in neomorphic activity with the production of D2HG. Panels show the conservation of the Arg100 residue across species to yeast. Additionally, the catalytic sites of IDH1 and IDH2 are highly homologous, as shown by complete homology neighboring the Arg100 and Arg140 residue in IDH1 and IDH2, respectively. MTS, mitochondrial targeting sequence.

(B) Comparison of WT and variant (Arg100Gln) protein are shown in ribbon rendering from  $t = 75$  ns during simulation (WT is blue and p.Arg100Gln is red). RMSD change over time for IDH1 WT and p.Arg100Gln variant is shown. Root-mean-square fluctuation (RMSF) per residue for IDH1 WT and p.Arg100Gln variant is shown.

(C) View of the catalytic pocket in IDH1/2 WT and p.Arg100Gln/p.Arg140Gln showing loss of hydrogen bonds due to mutation of the conserved arginine residues in both proteins.

correlate with decreased catalytic efficiencies, which have been confirmed experimentally.<sup>19,20</sup>

The IDH1 p.Arg100Gln variant has been shown to result in the production of low levels of D2HG *in vitro* (approaching the limit of detection). Therefore, we wanted to determine whether this germline variant could lead to a measurable increase in D2HG or other metabolites in plasma or urine, which could be detected by organic acid analysis *in vivo*. Organic acids (including 2-hydroxyglutarate, 2-oxoglutarate, and citrate) in urine and plasma were prepared by stable isotope dilution for capillary gas chromatography-mass spectrometry (GC-MS) analysis as oximated, silyl- derivatives.<sup>21</sup> Quantification of analytes was performed by comparing measured peak areas of quantifying ions on the GC-MS against unique quantifying ions of known concentrations of isotope-labeled internal standards. Six-point calibration curves were run for each quan-

tified analyte each time a new pentadecanoic acid (PDA) internal standard was prepared and renewed at least every 6 months. Plasma-free fatty acids (i.e., phytanic acid) were quantified by stable isotope dilution for GC-MS analysis as previously described.<sup>22</sup>

In these individuals, levels of urinary 2-hydroxyglutarate, citrate, and 2-oxoglutaric acid were within normal reference ranges, with the exception of slightly elevated 2-hydroxyglutarate levels in the proband at 35.2 mmol/mol creatinine (reference range: 1.3–13.9 mmol/mol creatinine) (Table 1). Plasma glutamine, glutamate, citrate, and 2-oxoglutarate levels were normal in tested individuals (Table 1). Because the alpha-hydroxylation of phytanic acid (a branched-chain fatty acid) is 2-oxoglutarate dependent, we examined levels of phytanic acid in plasma; however, no elevations were detected in the one individual who had this testing

**Table 1. Biochemical testing performed on urine and plasma in the proband, half-brother, and mother**

Metabolite	Proband	Half-brother	Mother	Reference Range or Units
Urinary 2-hydroxyglutarate	<u>35.2</u>	10.4	10.5	1.3–13.9 mmol/mol creatinine
Urinary citrate	259.1	141	262	120–582 mmol/mol creatinine
Urinary 2-oxoglutaric acid	20.7	NP	NP	2.4–94.8 mmol/mol creatinine
Plasma glutamine	NP	612	461	2–17 years: 329–976 nmol/mL ≥ 18 years: 371–957 nmol/mL
Plasma glutamate	NP	24	35	2–17 years: 22–131 nmol/mL ≥ 18 years: 13–113 nmol/mL
Plasma citrate	NP	398	NP	nmol/mL (non-clinical)
Plasma 2-oxoglutarate	NP	9.7	NP	nmol/mL (non-clinical)
Plasma Phytanic acid	NP	NP	0.68	normal < 9.88 mmol/mL

Values falling outside the reference range are underlined. NP, not performed.

performed (Table 1). Additional testing was unable to be performed as the family was lost to follow-up.

Next we wanted to analyze if p.Arg100Gln has functional consequences in the cell in which it is expressed. One hallmark of *IDH* mutant tumors is a global hypermethylation. Due to limited tumoral tissue and low tumoral cellularity, we were unable to obtain sufficient DNA from the proband's tumor for subsequent methylation analyses. Thus, in order to determine whether the p.Arg100Gln variant leads to an *IDH* mutant phenotype *in vivo*, we performed genome-wide methylation analysis on a p.Arg100Gln mutant diffuse astrocytoma from an unrelated individual. Briefly, DNA was extracted from the low-grade diffuse astrocytoma formalin fixed paraffin embedded (FFPE) tumor specimen, which had a tumor percentage of ~80%. *IDH* mutation analysis by Sanger sequencing confirmed the c.299G>A, p.Arg100Gln variant in *IDH1* at ~40% variant allele frequency (Figure 3A). Subsequently we performed genome-wide DNA methylation profiling with the 850k Illumina methylation array, according to the manufacturer's instructions (Illumina). Idat-files were uploaded to the brain tumor classifier, version v11b4. In the classifier, the sample received the highest calibrated scores for the "methylation class *IDH* glioma, subclass high grade astrocytoma" (0.745) and "methylation class *IDH* glioma, subclass astrocytoma" (0.250). We computed a t-distributed stochastic neighbor embedding (t-SNE) of the p.Arg100Gln mutant tumor together with reference cases for different glioma subtypes taken from the reference set of the brain tumor classifier,<sup>23</sup> including known *IDH* mutation-positive and WT cases, via the R package Rtsne<sup>24</sup> using the methylation levels of the 20,000 most variable CpG sites in the dataset according to standard deviation, 3,000 iterations, and a perplexity value of 10. The p.Arg100Gln mutant tumor was found to cluster together with *IDH* mutant tumors (Figure 3B). These analyses reveal that the p.Arg100Gln mutant brain tumor shares genome-wide methylation changes similar to other *IDH* mutant tumors. This result shows that the pArg100Gln

mutation, although producing less D2HG, is sufficient to induce the methylation phenotype that is characteristic for *IDH* mutant tumors and thought to be the main driver of tumorigenesis.

The mastoid process is rudimentary in the neonatal skull, with only the antrum present by 34 weeks.<sup>25</sup> The mastoid largely forms postnatally, and there are three phases of mastoid pneumatization and development.<sup>25</sup> In the first year, there is a period of rapid pneumatization.<sup>25</sup> During the second stage, from 1 to 6 years, there is a linear pattern of aeration followed by a third, slower phase, that continues until puberty when the mastoid reaches adult size.<sup>25</sup>

While somatic mosaic *IDH* variants in cartilaginous tumors were initially identified in individuals with Ollier or Mafucci syndrome, an estimated 70% of sporadic enchondromas and primary chondrosarcomas also contain *IDH* variants. In contrast, we know of no prior examples of germline *IDH* variants associated with cartilaginous tumors. The pathogenicity of *IDH* variants has been well-described for more common variants. We have previously quantified D2HG production in cells and found that *IDH1* p.Arg100Gln results in very low levels of D2HG.<sup>19</sup> Ward et al.<sup>7</sup> have shown that variant *IDH1* forms heterodimers with WT *IDH1*, leading to enhanced production of D2HG. It has been proposed that heterodimerization provides the variant *IDH1* subunit with a local source of  $\alpha$ -KG that can then be metabolized to D2HG. It is therefore interesting that we saw increased hydrogen bonding between WT and p.Arg100Gln monomers, suggesting a stronger association in the heterodimeric form in our simulations.

However, in cases of very high  $K_M$  values, such as in the case of p.Arg100Gln *IDH1*, it is questionable whether the reaction producing D2HG is physiologically relevant, even in heterodimeric form.<sup>20</sup> Previous *in vitro* enzyme assays yielded the highest  $K_M$ ,  $\alpha$ KG values for p.Arg100Gln *IDH1*, compared to variants affecting the *IDH1* R132 residue.<sup>19</sup> Interestingly, p.Arg100Gln *IDH1* exhibits increased  $K_M$  values both for isocitrate and  $\alpha$ KG,

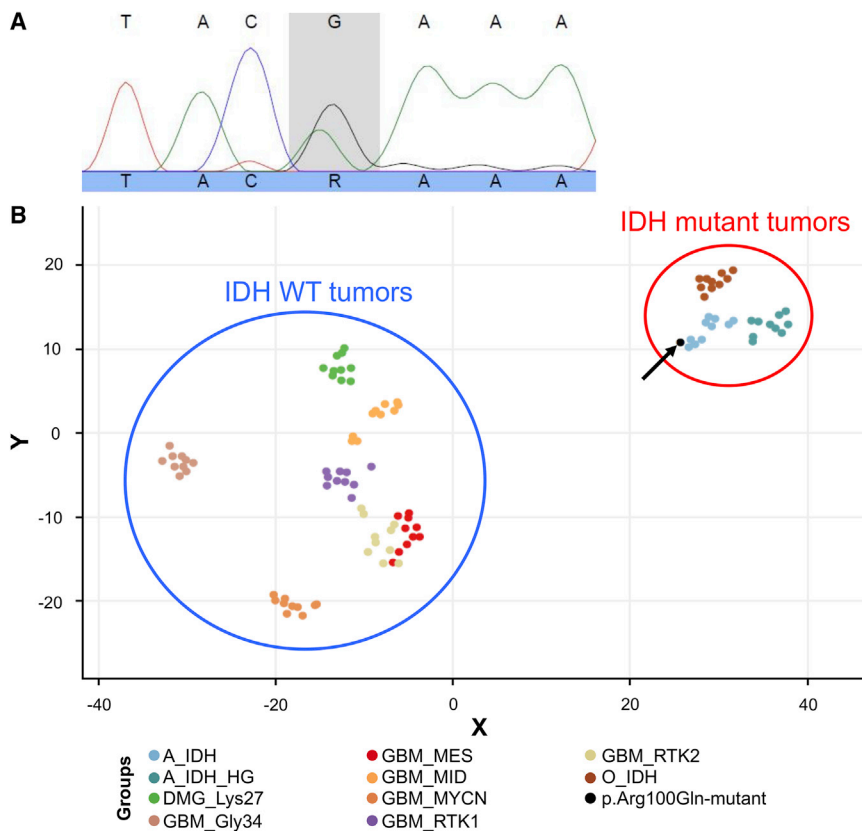


**Figure 3. Sanger Sequencing and Genome-wide Methylation Profiling of an IDH1 p.Arg100Gln Mutant Low Grade Diffuse Astrocytoma**

(A) Sanger sequencing trace showing the *IDH1* p.Arg100Gln mutation in low-grade diffuse astrocytoma case.

(B) t-SNE of DNA methylation profiles of the p.Arg100Gln mutant case together with cases for different glioma subtypes (each  $n = 10$ ) randomly selected from the reference set of the brain tumor classifier. Group name abbreviations: A\_IDH, methylation class IDH glioma, subclass astrocytoma; A\_IDH\_HG, methylation class IDH glioma, subclass high grade astrocytoma; DMG\_Lys27, methylation class diffuse midline glioma H3 p.Lys27Met mutant; GBM\_Gly34, methylation class glioblastoma, IDH wild-type, H3.3 Gly34 mutant; GBM\_MES, methylation class glioblastoma, IDH wild-type, subclass mesenchymal; GBM\_MID, methylation class glioblastoma, IDH wild-type, subclass midline; GBM\_MYCN, methylation class glioblastoma, IDH wild-type, subclass MYCN; GBM\_RTK1, methylation class glioblastoma, IDH wild-type, subclass RTK I; GBM\_RTK2, methylation class glioblastoma, IDH wild-type, subclass RTK II; O\_IDH, methylation class IDH glioma, subclass 1p/19q codeleted oligodendroglioma.

correlating with decreased catalytic efficiency for both reactions.<sup>19</sup>

Quantitative differences in the production of D2HG have been shown to produce different downstream biological effects. For instance, in a glioma model, activating variants in *IDH1* that produce low levels of D2HG appear to promote proliferation, while high levels result in reduced proliferation.<sup>19</sup> While the concentration of D2HG produced by the p.Arg100Gln variant is very low, glioma tumors and cells with this variant appear to have the same mutant IDH phenotype as those with more common variants.<sup>19</sup> The extent of differentiation blockade is also dependent on levels of D2HG, with higher amounts resulting in greater inhibition of  $\alpha$ -KG-dependent dioxygenases and greater impairment of cellular differentiation.<sup>1</sup> The amount of D2HG that is produced and tissue specific dependency on IDH isozymes for energy production likely determine the disease phenotype.<sup>1</sup> This is supported by the fact that neomorphic *IDH1* and *IDH2* variants are found at different frequencies in different cancers and in some rare inherited conditions.

Variants in *PTPN11* can also cause autosomal dominant metachondromatosis (MIM: 151623). These disorders are characterized by multiple exostoses and multiple enchondromatosis involving the long bones, metacarpals, pelvis, ribs, and scapula and carry a small risk of transformation to chondrosarcoma. Ollier disease and Maffucci syndrome are associated with the development of multiple enchon-

dromas, in addition to hemangiomas in Maffucci syndrome.<sup>4</sup> Most individuals have somatic variants in *IDH1* (Arg132 alterations), with relatively few cases with *IDH2* variants (Arg140 and Arg172).<sup>4</sup> While unusual, chondrosarcomas of the skull base have been described in Ollier disease and Maffucci syndrome, but they have not specifically involved the mastoid, and bilateral chondrosarcomas in these syndromes have not been reported.<sup>26</sup> Symmetric enchondromas within the metaphyses of the tubular long bones have been described in genochondromatosis (MIM: 137360), which shows dominant inheritance in some families.<sup>3</sup> However, skull lesions have not been described in these individuals and the genetic basis of this disease has not been identified.

Chondrosarcomas affecting the mastoid are rare<sup>27</sup> but may more commonly involve other sites within the temporal bone. One recent study of chondrosarcomas of the skull base found a high rate of somatic *IDH1* variants.<sup>28</sup> Overall, *IDH1* variants were found in 85.7% (24/28) of tumors in this region, but none were found in tumors involving the facial bones (mainly maxillary bone and nasal cartilage sites,  $n = 9$ ).<sup>28</sup> Of the *IDH1* mutation-positive skull base chondrosarcomas, all involved Arg132, with the most common variants being p.Arg132Cys (62.5%), p.Arg132Gly (16.7%), and p.Arg132Leu (12.5%).<sup>28</sup> Chondrosarcomas of the skull base were most commonly observed in the petrous part of the temporal bone.<sup>28</sup> The petrous bone forms part of the posterior of

the chondrocranium, which is derived from the paraxial mesoderm, whereas the mastoid forms part of the tympanic cavity, which develops from neural crest cells within the first pharyngeal pouch.<sup>28</sup> In addition, the petrous bone forms via enchondral ossification, while the mastoid forms by membranous ossification, suggesting that differences in both embryonic origin as well as mode of ossification may play a role in the development of these tumors in the context of different IDH variants.<sup>28</sup>

It is possible that the production of low levels of D2HG by the p.Arg100Gln variant could impede membranous ossification and promote tumor formation within embryonic cartilage rests within the mastoid. We have shown that this variant is sufficient to drive a global methylation phenotype similar to other IDH variants within a p.Arg100Gln mutant astrocytoma. While this observation is certainly relevant for p.Arg100Gln mutant brain tumors, it is unclear whether this can be extrapolated to chondrosarcomas, and further work will be necessary. In the family described here, no other malignancies were noted, and skeletal surveys showed no evidence of enchondromas or other bony lesions at other locations in the body, suggesting that the mastoid may be uniquely sensitive to the perturbations caused by this variant. The timing of the development of these chondrosarcomas in this family is intriguing in that they arose in all three affected individuals around puberty, when the development of the mastoid is completed. Additional study, including testing of individuals with similar presentations, will be necessary to confirm this finding and further elucidate the pathobiology of this tumor entity.

## Data and code availability

The whole-exome sequencing datasets supporting the current study have not been deposited in a public repository because these data were collected by the clinical reference testing institution without patient consent to do so. EPIC array data are available from the corresponding author on request.

## Supplemental Information

Supplemental information can be found online at <https://doi.org/10.1016/j.xhgg.2020.100006>.

## Acknowledgments

We would like to thank the subjects and their family for participating in this study. This work was made possible through support provided by the Mayo Clinic Center for Individualized Medicine (CIM) through the CIM Investigative and Functional Genomics Program.

## Declaration of interests

A patent for a “DNA-methylation based method for classifying tumor species of the brain” has been applied for by

the Deutsches Krebsforschungszentrum Stiftung des öffentlichen Rechts and Ruprecht-Karls-Universität Heidelberg (EP16710700.2A, CA2978843A, US15/551,573) on which A.v.D. is mentioned as an inventor. The other authors have no other conflicts of interest.

Received: May 19, 2020

Accepted: July 21, 2020

## Web resources

Catalogue Of Somatic Mutations In Cancer (COSMIC), <https://cancer.sanger.ac.uk/cosmic>

Genome Aggregation Database (gnomAD), <https://gnomad.broadinstitute.org/>

German Cancer Research Center (DKFZ) DNA methylation-based classification, <https://www.moleculareuropathology.org/mnp-OMIM>, <https://www.omim.org/>

## References

1. Losman, J.-A., and Kaelin, W.G., Jr. (2013). What a difference a hydroxyl makes: mutant IDH, (R)-2-hydroxyglutarate, and cancer. *Genes Dev.* 27, 836–852.
2. Yang, H., Ye, D., Guan, K.-L., and Xiong, Y. (2012). IDH1 and IDH2 mutations in tumorigenesis: mechanistic insights and clinical perspectives. *Clin. Cancer Res.* 18, 5562–5571.
3. Pansuriya, T.C., Kroon, H.M., and Bovée, J.V.M.G. (2010). Enchondromatosis: insights on the different subtypes. *Int. J. Clin. Exp. Pathol.* 3, 557–569.
4. Pansuriya, T.C., van Eijk, R., d’Adamo, P., van Ruler, M.A.J.H., Kuijjer, M.L., Oosting, J., Cleton-Jansen, A.-M., van Oosterwijk, J.G., Verbeke, S.L.J., Meijer, D., et al. (2011). Somatic mosaic IDH1 and IDH2 mutations are associated with enchondroma and spindle cell hemangioma in Ollier disease and Maffucci syndrome. *Nat. Genet.* 43, 1256–1261.
5. Kranendijk, M., Struys, E.A., van Schaftingen, E., Gibson, K.M., Kanhai, W.A., van der Knaap, M.S., Amiel, J., Buist, N.R., Das, A.M., de Klerk, J.B., et al. (2010). IDH2 mutations in patients with D-2-hydroxyglutaric aciduria. *Science* 330, 336, 336.
6. Bonnet, C., Thomas, L., Psimaras, D., Bielle, F., Vauléon, E., Loiseau, H., Cartalat-Carel, S., Meyronet, D., Dehais, C., Honnorat, J., et al. (2016). Characteristics of gliomas in patients with somatic IDH mosaicism. *Acta Neuropathol. Commun.* 4, 31.
7. Ward, P.S., Cross, J.R., Lu, C., Weigert, O., Abel-Wahab, O., Levine, R.L., Weinstock, D.M., Sharp, K.A., and Thompson, C.B. (2012). Identification of additional IDH mutations associated with oncometabolite R(-)-2-hydroxyglutarate production. *Oncogene* 31, 2491–2498.
8. Pusch, S., Sahm, F., Meyer, J., Mittelbronn, M., Hartmann, C., and von Deimling, A. (2011). Glioma IDH1 mutation patterns off the beaten track. *Neuropathol. Appl. Neurobiol.* 37, 428–430.
9. Frisch, C.D., Inwards, C.Y., Lalich, I.J., Carter, J.M., and Neff, B.A. (2016). Atypical cartilaginous tumor/chondrosarcoma, grade 1, of the mastoid in three family members: A new entity. *Laryngoscope* 126, E310–E313.
10. Asmann, Y.W., Middha, S., Hossain, A., Baheti, S., Li, Y., Chai, H.-S., Sun, Z., Duffy, P.H., Hadad, A.A., Nair, A., et al. (2012). TREAT: a bioinformatics tool for variant annotations and

- visualizations in targeted and exome sequencing data. *Bioinformatics* 28, 277–278.
11. McKenna, A., Hanna, M., Banks, E., Sivachenko, A., Cibulskis, K., Kernytzky, A., Garimella, K., Altshuler, D., Gabriel, S., Daly, M., and DePristo, M.A. (2010). The Genome Analysis Toolkit: a MapReduce framework for analyzing next-generation DNA sequencing data. *Genome Res.* 20, 1297–1303.
  12. Kocher, J.-P.A., Quest, D.J., Duffy, P., Meiners, M.A., Moore, R.M., Rider, D., Hossain, A., Hart, S.N., and Dinu, V. (2014). The Biological Reference Repository (BioR): a rapid and flexible system for genomics annotation. *Bioinformatics* 30, 1920–1922.
  13. Sobreira, N.L.M., Cirulli, E.T., Avramopoulos, D., Wohler, E., Oswald, G.L., Stevens, E.L., Ge, D., Shianna, K.V., Smith, J.P., Maia, J.M., et al. (2010). Whole-genome sequencing of a single proband together with linkage analysis identifies a Mendelian disease gene. *PLoS Genet.* 6, e1000991.
  14. Bowen, M.E., Boyden, E.D., Holm, I.A., Campos-Xavier, B., Bonafé, L., Superti-Furga, A., Ikegawa, S., Cormier-Daire, V., Bovée, J.V., Pansuriya, T.C., et al. (2011). Loss-of-function mutations in PTPN11 cause metachondromatosis, but not Ollier disease or Maffucci syndrome. *PLoS Genet.* 7, e1002050.
  15. Kumar, P., Henikoff, S., and Ng, P.C. (2009). Predicting the effects of coding non-synonymous variants on protein function using the SIFT algorithm. *Nat. Protoc.* 4, 1073–1081.
  16. Adzhubei, I.A., Schmidt, S., Peshkin, L., Ramensky, V.E., Gerasimova, A., Bork, P., Kondrashov, A.S., and Sunyaev, S.R. (2010). A method and server for predicting damaging missense mutations. *Nat. Methods* 7, 248–249.
  17. Kircher, M., Witten, D.M., Jain, P., O’Roak, B.J., Cooper, G.M., and Shendure, J. (2014). A general framework for estimating the relative pathogenicity of human genetic variants. *Nat. Genet.* 46, 310–315.
  18. Mellai, M., Caldera, V., Annovazzi, L., and Schiffer, D. (2013). The Distribution and Significance of IDH Mutations in Gliomas. In *Evolution of the Molecular Biology of Brain Tumors and the Therapeutic Implications*, T. Lichtor, ed. (Intech Open Science), pp. 299–341.
  19. Pusch, S., Schweizer, L., Beck, A.-C., Lehmler, J.-M., Weissert, S., Balss, J., Miller, A.K., and von Deimling, A. (2014). D-2-Hydroxyglutarate producing neo-enzymatic activity inversely correlates with frequency of the type of isocitrate dehydrogenase 1 mutations found in glioma. *Acta Neuropathol. Commun.* 2, 19.
  20. Avellaneda Matteo, D., Grunseth, A.J., Gonzalez, E.R., Anselmo, S.L., Kennedy, M.A., Moman, P., Scott, D.A., Hoang, A., and Sohl, C.D. (2017). Molecular mechanisms of isocitrate dehydrogenase 1 (IDH1) mutations identified in tumors: The role of size and hydrophobicity at residue 132 on catalytic efficiency. *J. Biol. Chem.* 292, 7971–7983.
  21. Rinaldo, P. (2008). Organic Acids. In *Laboratory Guide to the Methods in Biochemical Genetics*, N. Blau, M. Duran, and K.M. Gibson, H. Berlin, ed. (Berlin, Heidelberg: Springer), pp. 137–169.
  22. Lagerstedt, S.A., Hinrichs, D.R., Batt, S.M., Magera, M.J., Rinaldo, P., and McConnell, J.P. (2001). Quantitative determination of plasma c8-c26 total fatty acids for the biochemical diagnosis of nutritional and metabolic disorders. *Mol. Genet. Metab.* 73, 38–45.
  23. Capper, D., Jones, D.T.W., Sill, M., Hovestadt, V., Schrimpf, D., Sturm, D., Koelsche, C., Sahm, F., Chavez, L., Reuss, D.E., et al. (2018). DNA methylation-based classification of central nervous system tumours. *Nature* 555, 469–474.
  24. Krijthe, J.H. (2015). Rtsne: T-Distributed Stochastic Neighbor Embedding using a Barnes-Hut Implementation. <https://github.com/jkrijthe/Rtsne>.
  25. Cinamon, U. (2009). The growth rate and size of the mastoid air cell system and mastoid bone: a review and reference. *Eur. Arch. Otorhinolaryngol.* 266, 781–786.
  26. Ranger, A., and Szymczak, A. (2009). Do intracranial neoplasms differ in Ollier disease and maffucci syndrome? An in-depth analysis of the literature. *Neurosurgery* 65, 1106–1113, discussion 1113–1115.
  27. Zhao, E.E., Liu, Y.F., Oyer, S.L., Smith, M.T., and McRackan, T.R. (2019). Chondrosarcoma Arising in the Mastoid Involving the Intratemporal Facial Nerve. *JAMA Otolaryngol. Head Neck Surg.* 145, 392–393.
  28. Tallegas, M., Miquelestorena-Standley, É., Labit-Bouvier, C., Badoual, C., Francois, A., Gomez-Brouchet, A., Aubert, S., Collin, C., Tallet, A., and de Pinieux, G. (2019). IDH mutation status in a series of 88 head and neck chondrosarcomas: different profile between tumors of the skull base and tumors involving the facial skeleton and the laryngotracheal tract. *Hum. Pathol.* 84, 183–191.